Controlled surface modification to revive shallow NV^- centers

J. Neethi Neethirajan,[†] T. Hache,[†] D. Paone,[†,‡] D. Pinto,[†,¶] A. Denisenko,[‡] R. Stöhr,[‡] P. Udvarhelyi,[§,‖] A. Pershin,[§,‖] A. Gali,[§,‖] J. Wrachtrup,[‡,†] K. Kern,[†,¶] and A. Singha[*,†]

†*Max Planck Institute for Solid State Research, 70569 Stuttgart, Germany*

‡*3rd Institute of Physics and Research Center SCoPE, University Stuttgart*

¶*Institute de Physique, École Polytechnique Fédérale de Lausanne*

§*Wigner Research Centre for Physics, Institute for Solid State Physics and Optics, Budapest, POB 49, H-1525, Hungary*

‖*Department of Atomic Physics, Institute of Physics, Budapest University of Technology and Economics, Műegyetem rakpart 3., H-1111, Budapest, Hungary*

E-mail: a.singha@fkf.mpg.de

Abstract

Near-surface negatively charged nitrogen-vacancy (NV) centers hold excellent promises for nanoscale magnetic imaging and quantum sensing. However, they often experience charge state instabilities leading to strongly reduced fluorescence and NV-coherence time, which negatively impact magnetic imaging sensitivity. This occurs even more severely at 4 K and ultra high vacuum (UHV, $p = 2 \cdot 10^{-10}$ mbar). We demonstrate that *in situ* adsorption of H_2O on the diamond surface allows partial recovery of the shallow NV-sensors. Combining these with band bending calculations, we conclude

that controlled surface treatments are essential for implementing NV-based quantum sensing protocols at cryogenic UHV conditions.

Introduction

The nitrogen-vacancy (NV) center in diamond is a leading contender for quantum information processing and nanoscale quantum sensing.[1,2] The application of NV center as solid state quantum sensor spans a wide range, including the investigation of 2D Van der Waals magnets of unique spin textures,[3–5] unraveling superconducting properties at the nanoscale,[6–8] highly sensitive NMR studies of organic molecules,[9–12] and recent works of readout and control down to the level of single magnetic molecules.[13] Notably, all NV-based sensing schemes rely on the unique electronic spin configuration of the negatively charged defect center (NV^-) and are realized by recording its spin dependent fluorescence.[14] However, in near-surface NV centers it has been shown that several unavoidable interactions often lead to charge transfers resulting in the formation of the neutral NV^0 state. This leads to undesired fluorescence quenching and significant reduction in NV-coherence time.[15–20] NV centers implanted at depths > 10 nm can retain a stable NV^- state,[19] whereas shallow NVs exhibit charge state instabilities often evidenced as fluorescence blinking.[19,20] Despite few attempts to mitigate the issue of charge-state instabilities,[21–25] a working recipe is still missing for stabilizing shallow NV centers without compromising on their performance. In addition, most of these approaches are yet to be explored (a) for single NV centers in a diamond nanopillar, a geometry especially attractive for scanning NV-magnetometry,[26] and (b) for operations under extreme measurement conditions of ultra high vacuum (UHV) in combination with low temperatures (4 K), where an abundance of delicate atomic-scale spin systems and physical processes are often investigated.[27–31]

Here, we report partial recovery of the optical and spin properties in isolated shallow-NV centers hosted within individual diamond nanopillars, upon controlled surface modifications

performed in UHV conditions. Combining these with band bending calculations, we reveal the correlation between the local changes in the electronic structure of the surface and the charge state stability of the NV center.

Results and discussion

All measurements are obtained from a diamond nanopillars membrane (Fig. 1)[32] under two different conditions, (a) ambient temperature and pressure (NTP) and (b) LT-UHV (T = 4 K, p = $2 \cdot 10^{-10}$ mbar). The NV centers are formed at a depth of about (8 ± 3.1) nm by irradiating with 5 keV ^{15}N ions (see Methods).[33] The NVs are optically excited by a 515 nm laser. The resulting NV fluorescence is recorded in two ways: (a) after passing through a long pass (LP) 650 nm filter the signal is collected by the the detection optics (dual APDs mounted in a Hanbury Brown and Twiss geometry) for autocorrelation measurements and (b) after passing through an LP-550 nm filter the signal is recorded by a spectrometer for emission spectroscopy (see Fig. 1, Methods, and SI-1 for further experimental details).[34,35] Notably, the nanopillar structure on the diamond surface enhances the photon collection efficiency from single NV centers.

The fluorescence yield of the NV center strongly depends on its charge states which are characterized by their distinct energy level distributions.[19] In shallow NV centers, spontaneous charge state conversions are often triggered by local imperfections of the diamond surface such as, presence of surface adsorbates, uncontrolled creation of vacancy clusters and charge traps (created during NV-growth process[36]). The unavoidable interactions and charge transfers with such surface-imperfections result in a correlated reduction in the optical and spin properties of the shallow NV centers.[37,38] In order to verify the environmental impact on the NV center's charge state, we employed measurements of the emission spectra, autocorrelation and optically detected magnetic resonance (ODMR) on the same NV centers under NTP and LT-UHV conditions.

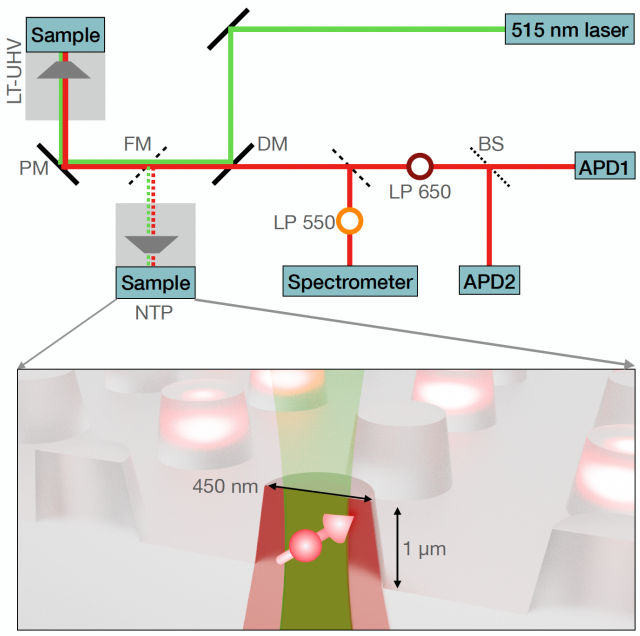

Figure 1: Schematic illustration of the experimental setup. FM: flip mirror, PM: piezo mirror, DM: dichroic mirror, BS: beamsplitter. Shallow NV centers are hosted in diamond nanopillars. The pillar structure enhances the photon collection efficiency from single NV centers.

An NV^- center spectrum is characterized by a zero-phonon line (ZPL) at 637 nm and a phonon side band with a maximum emission intensity at 690 nm.[39] In contrast, NV^0 centers are characterized by a ZPL at 575 nm and have a maximum in the phonon side band at 640 nm.[39] Notably, we obtained spectroscopic signatures of the NV^- charge state from NTP measurements (black spectrum in Fig. 2(a)). Instead, under LT-UHV conditions the same NV center exhibits a ZPL at 575 nm and a phonon side band peak at 630 nm which confirms a strong contribution from an NV^0 population (red spectrum, Fig. 2(a)). This significant modification of the emission spectra reveals a charge state conversion of the NV center at LT-UHV conditions.

The absence of the NV^- center under LT-UHV conditions is further supported by our auto-correlation measurements, as depicted in Fig. 2(b) for a representative single NV center. At NTP (black curve), we observe a clear antibunching dip with $g^{(2)} = 0.2$. Note that the slight increase of the auto-correlation signal just before the dip indicates a significant

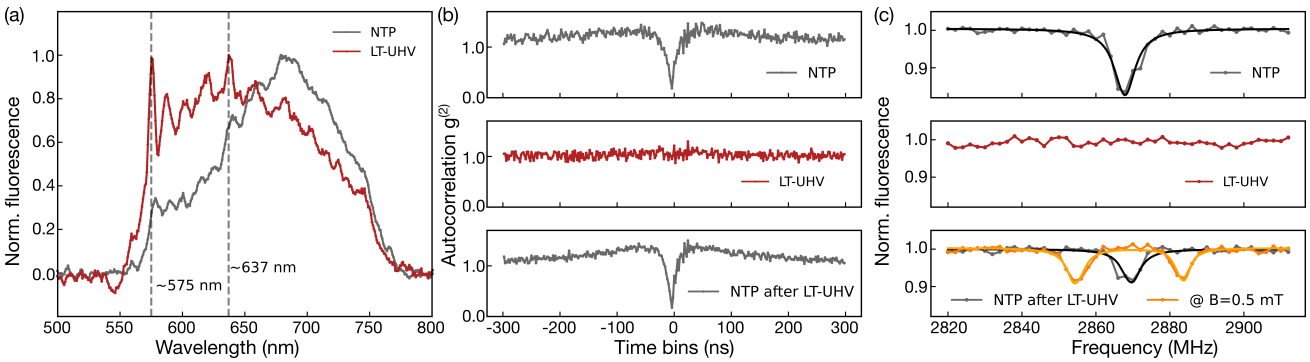

Figure 2: Compared to the measurements under ambient conditions, LT-UHV induces dramatic degradation of the optical and spin properties of the shallow NV centers, as demonstrated by (a) emission spectra, (b) autocorrelation and (c) ODMR measurements (dots: measurements, solid lines: Lorentzian fits). All measurements are performed on the same NV implanted at 8 ± 3 nm from the surface (hereafter called as NV #1). Pi-pulse lengths used for the pulsed-ODMR measurements in (c) are as follows: 250 ns (upper panel), 275 ns (middle panel), and 250 ns (lower panel, without field), 290 ns (lower panel, with field).

NV^- population, which can be modelled as a three-level system.[40] In stark contrast, the anti-bunching feature completely vanishes under LT-UHV conditions (red curve), which indicates that the majority of the NV^- contribution is diminished due to charge state instabilities, as also realised from emission spectroscopy.[41] Notably, the use of the LP650 filter blocks majority of the emission from the NV^0, thereby featuring no autocorrelation signature for this case.

The distinct electronic and spin properties of the NV^- and NV^0 centers, further provide a direct evidence of the NV charge state under the two measurement conditions, in terms of electron spin resonance measurements (ODMR spectroscopy). The NV^- center forms a spin triplet with a zero field splitting of 2.87 GHz in the ground state which is measured as a sharp ODMR line.[14] By applying an external magnetic field this resonance is split due to the Zeeman dependence of the sublevels.

In contrast, the NV^0 center forms a doublet ground state without any spin-dependent fluorescence response. As shown in Fig. 2(c) the measurements at ambient conditions exhibit the expected resonance at 2.87 GHz with 18 % contrast (black spectrum).[14,42] This resonance completely vanishes under the LT-UHV condition (red spectrum), which only recovers in a

subsequent measurement performed at ambient condition (grey and orange spectra exhibiting 9 % ODMR contrast). The ODMR measured at NTP with 1.4 mT external magnetic field further exhibits the expected Zeeman splitting of the $\mathfrak{m}_s = \pm 1$ levels as a direct fingerprint of the NV^- state. Note that some NVs have been observed to survive the extreme measurement conditions of LT-UHV, possibly due to their larger implantation depths (see Fig. S6 for additional measurements). Note that the same π-pulse length has been used for all measurements in Fig.2 (c). We attribute the slight decrease in the ODMR contrast in the second measurement run under ambient condition to the possible change in the microwave (MW) wire positioning during transfers of the sample to and from the LT-UHV stage.

The combined experimental evidences obtained from emission spectroscopy, autocorrelation and ODMR measurement performed on the same NV centers under the two measurement conditions reveal a dramatic suppression of the NV^- population at LT-UHV for shallow implanted NVs. We attribute this to possible adsorption and desorption processes that occur under these extreme measurement conditions which lead to significant changes to the diamond surface, thus strongly affecting the near-surface NVs. Typical candidates which easily adsorb on surfaces at ambient conditions are water molecules. With the relatively large dipole moment of the water molecule ($\approx 1.85\,\mathrm{D}$),[43] a surface-adsorbed water layer at NTP is capable of inducing a strong static electric field which influences the charge state distribution of the NV defects.[22]

We further link the loss of ODMR contrast at LT-UHV to a change in band bending at the interface, which we describe through a combination of ab initio density functional theory (DFT) calculations and continuum electrostatic model. To this end, we consider the charge state dynamics of the NV centers in a bath of nearby electron traps and hole emitter defects, e.g., vacancy clusters. Our model incorporates the divacancy defects (V_2) as representative hole emitters together with the substitutional nitrogen (N_s) donors and NV defects, created during the ion implantation and subsequent annealing processes. The laser illumination generates mobile holes in the valance band through the $V_2^{(0)} \rightarrow V_2^{(-)} + \mathfrak{h}^{(+)}$

photo-ionization process. Owing to its large hole capture cross section of $3 \cdot 10^{-3}$ μm^2,[44] the NV center preferentially captures a mobile hole, created during the ionization-recombination dynamics inside the bath of hole emitters. This process causes the charge state instability and demolishes the optical initialization of the NV^- charge state. To be efficient, it requires a thermodynamically stable $V_2^{(0)}$ charge state, which is in turn affected by the band bending near the surface. Thus, the strength of band bending defines the depth of the region from the diamond surface, where the NV^- emitter is unstable. We model this band bending using realistic densities of defects and accumulated surface charges, and compare the charge transition level (CTL) energy of $V_2^{(0)}$ with the Fermi level as a function of the depth for a nitrogen doped sample, see Fig. 3.

The strength of band bending is deduced from the DFT calculations, see Fig.S7 and the Supplementary note for details. Our modeling reveals a large positive shift in the potential energy at the interface, associated with a dipole moment of the oxygenated surface. The water molecules, adsorbed at the diamond surface, partly compensate the surface dipole through an electron transfer. This translates into an overall moderate positive band bending, providing the region of instability for the shallow NV centers (i.e., a region where the CTL of $V_2^{(0)}$ is above the calculated Fermi level) of 5 nm at room temperature. Under the LT-UHV condition, the adsorbed water is released from the surface, and the instability region extends to around 12 nm. Controlled water dosing could therefore restore the strength of band bending at ambient conditions, but keep in mind a new charge distribution at low temperature, which results in a slower decay of the energy levels towards bulk, see Fig. 3. However, our calculations predict only a small increase in the critical depth to 6 nm at 4.7K. Hence, a revival of the ODMR contrast due to water dosing should occur for all but the shallowest NV centers.

In order to verify this and to mitigate the charge state instabilities under LT-UHV conditions in a controlled manner, we dosed purified water in UHV following several freezing-pumping-thaw cycles (see Methods). Subsequently we investigated the effects on the emission

spectrum, autocorrelation and ODMR by measuring on the same pre-characterized NV as shown in Fig. 4 (a)-(c). While the NV fluorescence in absence of water layer exhibits a strong NV^0 ZPL at 575 nm, the latter is significantly reduced upon H_2O dosing. From the direct comparison of the shift in the phonon side bands, it becomes evident that the deposited water layer helps to promote a stronger relative NV^- population (Fig. 4(a)). An equivalent change is also observed from the autocorrelation measurements, as illustrated in Fig. 4(b). Before water dosing, the NV center does not show any antibunching feature. However, upon water dosing, a clear antibunching dip is observed.

The partial recovery of the negative charge state of the NV center is also evident from the measured ODMR signals in Fig. 4(c). For an undosed sample, no resonance lines can be obtained. However, after dosing water onto the diamond surface a weak albeit noticeable ODMR signal with a contrast of ≈ 2 % is recorded in a stray magnetic field of 0.7 mT (see Fig. S3 and S4 for additional control measurements).

Notably, a full recovery of the NV^- charge state in LT-UHV environment is not yet achieved via water dosing as evidenced by the relatively low ODMR contrast. Nevertheless, the dosed H_2O layer clearly indicates a relative change in the charge state population of the NV defect center induced by adsorption of polar compounds on the diamond surface,

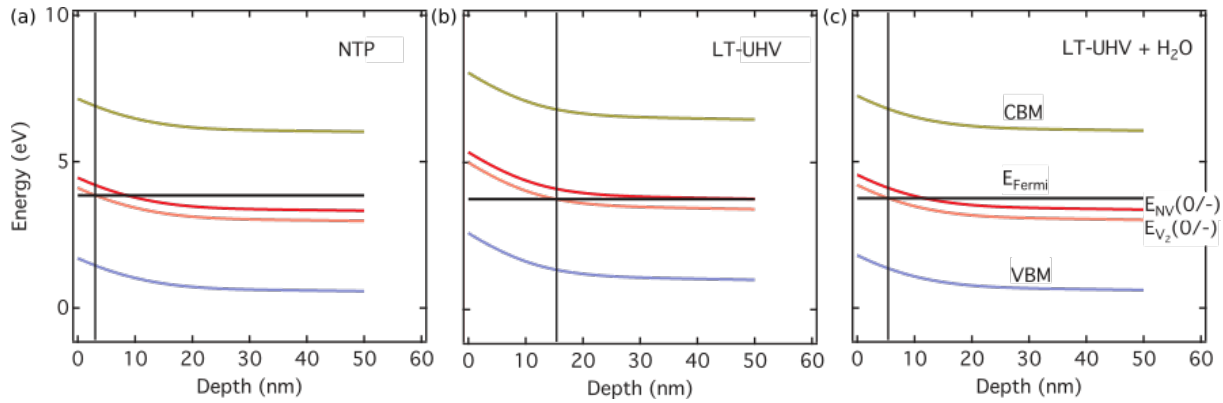

Figure 3: Simulated band bending as a function of depth from the diamond surface. (a) NTP condition with an adsorbed water layer on the surface. (b) LT-UHV condition without the effect of water. (c) Water dosing partially recovering the adsorbed surface layer. Dashed lines show the depth of instability for the NV emitter.

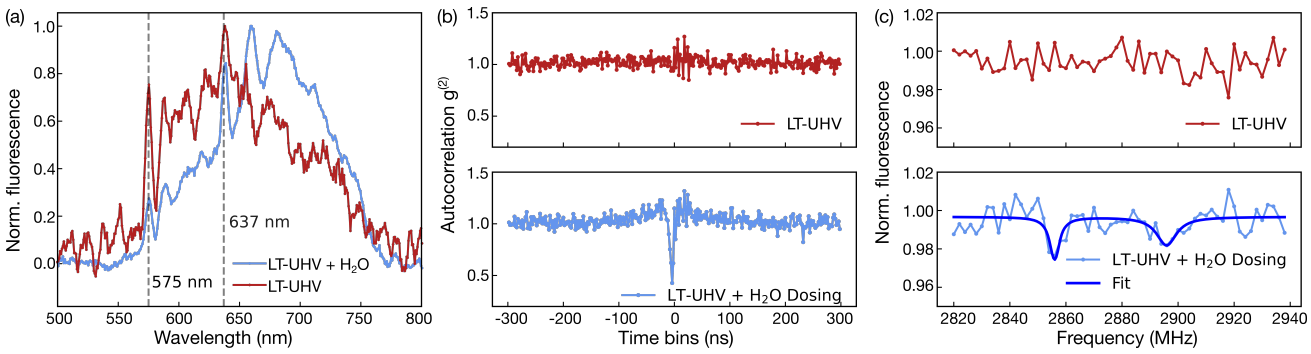

Figure 4: Revival of a shallow negatively charged NV center after water dosing in LT-UHV conditions, as evidenced by (a) characteristic changes in the emission spectrum, (b) re-appearance of antibunching dip in the autocorrelation signal, and (c) partial recovery of the ODMR signal. All measurements are performed on the same NV center implanted at 8±3 nm from the surface (NV #2). π-pulse length used for the pulsed-ODMR measurements in (c) are as follows: 120 ns (upper panel) and 150 ns (lower panel).

thus indicating controlled surface modification as a route for stabilizing shallow NVs for operations under LT-UHV conditions.

In conclusion, by combining autocorrelation measurements, ODMR, emission spectroscopy, and theoretical modeling, we confirm that NV centers undergo uncontrolled charge state modifications under extreme measurement conditions of UHV ($2 \cdot 10^{-10}$ mbar) and low temperatures (4.7 K). To the best of our knowledge, this is the first demonstration of instabilities of individual shallow NV centers within diamond nanopillars under these extreme measurement conditions. In addition, we also report that the NV centers exhibit a relative increase in the negative charge state upon an *in situ* deposition of water. The latter is expected to indirectly assist the NV charge state stabilization by hindering the hole emission from the nearby deep acceptor defects. Although the recovery of the negative charge state of the NVs are by far not comparable with that measured at NTP, our experiments clearly indicate that controlled surface treatments play a crucial role for using near-surface NV centers at LT-UHV conditions. Similar or better performance towards charge state stabilization might be achieved by controlled surface adsorption of inorganic layers (for instance *via* atomic layer deposition processes) or by preparing self-assemblies of robust molecular adsorbates. This

altogether brings sensing with shallow NV centers an important step forward, especially for investigating magnetic phenomena at nanometer length scales for samples which are prone to thermal instabilities or to chemical degradation under ambient condition, such as single molecular systems, thin film superconductors, and skyrmionic structures.

Methods

The NV layers were created by 2.5 keV, 5 keV and 10 keV nitrogen ion implantation (^{15}N) in an electronic grade (e6) CVD grown diamond. The beam energies of which defines the resulting NV center depth[45] (as shown in Fig. S1). The depths were simulated using "SRIM: The Stopping and Range of Ions in Matter" software.[46] Subsequently the diamond sample was annealed at 950 °C for two hours. The nanopillar structures were etched in the diamond for enhancing the photon collection efficiency.[47] All measurements reported in this work are performed with NVs implanted using 5 keV beam energy.

In order to perform measurements on a clean surface, the diamond membrane was cleaned and oxygen terminated by tri-acid boiling (HNO_3:HSO_4:$HClO_4$) at 200 °C for 6 hours. Afterwards, the diamond sample was glued onto a sample holder with a LT-UHV compatible varnish. After leaving it in the preparation chamber maintained at $2 \cdot 10^{-10}$ mbar for 12 hours, the sample was finally transferred into the cryogenic UHV measurement head ($< 2 \cdot 10^{-10}$ mbar).

The water dosing was performed in the preparation chamber of the LT-UHV setup. Distilled H_2O was utilized which has been purified by 5 rounds of a freeze-pump-thaw cycle.[48] A stainless steel needle which is connected to the water reservoir was placed in close proximity to the diamond surface and the H_2O was introduced through a high precision leak valve into the preparation chamber at $5 \cdot 10^{-7}$ mbar for 120 s. The dosing was performed directly after transferring the sample from the 4 K measurement head to the preparation chamber leading to the reasonable assumption of a cold diamond surface during dosing and, therefore,

strong adsorption of the water molecules. Subsequently, the sample was transferred into the LT-UHV environment for further measurements.

Ab initio calculations were performed using the PBE functional[49] in conjunction with the D2 dispersion correction scheme, implemented in the VASP package.[50] A projector augmented wave method with the kinetic energy cutoff of 370 eV was used. In our simulations, we used a slab of (100) diamond terminated with the hydrogen, hydroxyl, and ether surface groups.[51] This surface type causes a proper passivation of the dangling bonds, so that no surface states are present inside the band gap. By contrast, a realistic diamond surface contains a variety of defects (typically, of the acceptor defects such as carbon vacancies), while their density may even be increased during the ion implantation. To mimic the effect of the surface states in our calculations, we added a carboxyl group which develops a deep acceptor level inside the band gap of diamond. Next, the diamond slab was put in contact with 74 water molecules and 1.9 nm of vacuum in a simulation supercell of $1.0097 \times 1.0097 \times 5.3$ nm^3. A representative configuration was captured from the ab initio molecular dynamics trajectory of 10 ps, and was subsequently relaxed to a local minimum.

We calculate the depth dependence of the electric potential $V(x)$ inside diamond by numerically solving the boundary value problem of the Poisson's equation.

$$\frac{d^2V(x)}{dx^2} = \frac{-\rho(x)}{\varepsilon_0 \varepsilon_r}, \tag{1}$$

where $\rho(x)$ is the total charge density consisting of free space charges and defect acceptors and donors, ε_0 is the vacuum permittivity, $\varepsilon_r = 5.5$ is the relative permittivity of diamond. There are two boundary conditions to satisfy, firstly, the electric field vanishes in the bulk, secondly, the potential at the diamond surface is set according to the DFT calculation results. The accumulated surface charge density is calculated from the charge neutrality condition from the total charges inside the diamond. The band bending curves in Fig. 3 are simulated for accumulated surface charge densities of -0.041 e/nm^2, -0.051 e/nm^2 and -0.042 e/nm^2

for sub-figure (a), (b) and (c), respectively. We use the following characteristic energies in the bulk during the simulations, given relative to the valance band maximum. $E_C = 5.45$ eV, $E_{NV(0/-)} = 2.75$ eV, $E_{NV(+/0)} = 0.9$ eV, $E_{Ns(+/0)} = 3.75$ eV, $E_{V_2(+/0)} = 1.15$ eV, $E_{V_2(0/-)} = 2.4$ eV are the energy levels for the conduction band minimum, NV center acceptor and donor levels, substitutional nitrogen donor level, divacancy donor and acceptor levels, respectively. We assume Gaussian defect density profiles for the implantation, centered at 10 nm depth with a variance of 10 nm. The peak implanted defect concentrations are $\rho_{Ns} = 15$ ppm, $\rho_{NV} = 3$ ppm and $\rho_{V_2} = 3$ ppm. The acceptor and donor densities are calculated from the Fermi-Dirac statistics with respect to the Fermi level in bulk.

Acknowledgement

A.S. gratefully acknowledges IQST-YR grant from the Center for IQST, and Emmy Noether grant from the Deutsche Forschungsgemeinschaft (project no. 504973613). A.G. acknowledges the National Research, Development, and Innovation Office of Hungary (NKFIH) grant No. KKP129866 of the National Excellence Program of Quantum-coherent materials project and the Quantum Information National Laboratory supported by the Ministry of Culture and Innovation of Hungary, the EU QuantERA II MAESTRO project, and the Horizon Europe EIC Pathfinder QuMicro project (grant No. 101046911).

Author contribution

A.S., J.W., and K.K. conceived the idea. J.N.N, D. Paone, and T.H. performed the experiments. J.N.N, D.Paone, D.Pinto, and A.S. performed the data analysis. R.S. and A.D. designed and prepared the diamond nanopillar membrane. P.U., A.P., and A.G. performed the band bending calculations. D.Paone, T.H., and A.S. drafted the manuscript with contributions from all authors. A.S. supervised the project.

Supporting Information Available

The supporting information contains the details of the experimental setup and additional control measurements.

References

(1) Taylor, J. M.; Cappellaro, P.; Childress, L.; Jiang, L.; Budker, D.; Hemmer, P. R.; Yacoby, A.; Walsworth, R.; Lukin, M. D. High-sensitive diamond magnetometer with nanoscale resolution. *Nature Physics* **2008**, *4*, 810–816.

(2) Xu, Z.; Yin, Z.; Han, Q.; Li, T. Quantum information processing with closely-spaced diamond color centers in strain and magnetic fields. *Optical Materials Express* **2019**, *9*, 4654–4668.

(3) Sun, Q.-C.; Song, T.; Anderson, E.; Brunner, A.; Förster, J.; Shalomayeva, T.; Taniguchi, T.; Watanabe, K.; Gräfe, J.; Stöhr, R.; Xu, X.; Wrachtrup, J. Magnetic domains and domain wall pinning in atomically thin CrBr3 revealed by nanoscale imaging. *Nature Communications* **2021**, *12*, 1989.

(4) Thiel, L.; Wang, Z.; Tschudin, M. A.; Rohner, D.; Gutiérrez-Lezama, I.; Ubrig, N.; Gibertini, M.; Giannini, E.; Morpurgo, A. F.; Maletinsky, P. Probing magnetism in 2D materials at the nanoscale with single-spin microscopy. *Science* **2019**, *364*, 973–976.

(5) Hedrich, N.; Wagner, K.; Pylypovski, O. V.; Shields, B. J.; Kosub, T.; Sheka, D. D.; Makarov, D.; Maletinsky, P. Nanoscale mechanics of antiferromagnetic domain walls. *Nature Physics* **2021**, *17*, 574–577.

(6) Thiel, L.; Rohner, D.; Ganzhorn, M.; Appel, P.; Neu, E.; Müller, B.; Kleiner, R.; Koelle, D.; Malitensky, P. Quantitative nanoscale vortex imaging using a cryogenic quantum magnetometer. *Nature Nanotechnology* **2016**, *11*, 677–681.

(7) Pelliccione, M.; Jenkins, A.; Ovartchaiyapong, P.; Reetz, C.; Emmanouilidou, E.; Ni, N.; Jayich, A. C. B. Scanned probe imaging of nanoscale magnetism at cryogenic temperatures with a single-spin quantum sensor. *Nature Nanotechnology* **2016**, *11*, 700–705.

(8) Paone, D.; Pinto, D.; Kim, G.; Feng, L.; Kim, M.-J.; Stöhr, R.; Singha, A.; Kaiser, S.; Logvenov, G.; Keimer, B.; Wrachtrup, J.; Kern, K. All-optical and microwave-free detection of Meissner screening using nitrogen-vacancy centers in diamond. *Journal of Applied Physics* **2016**, *129*, 024306.

(9) Staudacher, T.; Shi, F.; Pezzagna, S.; Meijer, J.; Du, J.; Meriles, C. A.; Reinhard, F.; Wrachtrup, J. Nuclear Magnetic Resonance Spectroscopy on a (5-Nanometer)3 Sample Volume. *Science* **2013**, *339*, 561–563.

(10) Schmitt, S. et al. Submillihertz magnetic spectroscopy performed with a nanoscale quantum sensor. *Science* **2017**, *356*, 832–837.

(11) Boss, J. M.; Cujia, K. S.; Zopes, J.; Degen, C. L. Quantum sensing with arbitrary frequency resolution. *Science* **2017**, *356*, 837–840.

(12) Bucher, D. B.; Glenn, D. R.; Park, H.; Lukin, M. D.; ; Walsworth, R. L. Hyperpolarization-Enhanced NMR Spectroscopy with Femtomole Sensitivity Using Quantum Defects in Diamond. *Physical Review X* **2020**, *10*, 021053.

(13) Pinto, D.; Paone, D.; Kern, B.; Dierker, T.; Wieczorek, R.; Singha, A.; Dasari, D.; Finkler, A.; Harneit, W.; Wrachtrup, J.; Kern, K. Readout and control of an endofullerene electronic spin. *Nature Communications* **2020**, *11*, 6405.

(14) Jelezko, F.; Wrachtrup, J. Single defect centres in diamond: A review. *Physica Status Solidi* **2006**, *203*, 3207–3225.

(15) Sola-Garcia, M.; Meuret, S.; Coenen, T.; Polman, A. Electron Induced State Conversion in Diamond NV Centers Measured with Pump Probe Cathololuminescence Spectroscopy. *ACS Photonics* **2020**, *7*, 232–240.

(16) Grotz, B.; Hauf, M. V.; Dankerl, M.; Naydenov, B.; Pezzagna, S.; Meijer, J.; Jelezko, F.; Wrachtrup, J.; Stutzmann, M.; Reinhard, F.; Garrido, J. A. Charge state manipulation of qubits in diamond. *Nature Communications* **2012**, *10*, 729.

(17) Schreyvogel, C.; Polyakov, V.; Wunderlich, R.; Meijer, J.; Nebel, C. E. Active charge state control of single NV centres in diamond by in-plane Al-Schottky junctions. *Scientific Reports* **2015**, *5*, 12160.

(18) Ofori-Okai, B. K.; Pezzagna, S.; Chang, K.; Loretz, M.; Schirhagl, R.; Tao, Y.; Moores, B. A.; Groot-Berning, K.; Meijer, J.; Degen, C. L. Spin properties of very shallow nitrogen vacancy defects in diamond. *Phys. Rev. B* **2012**, *86*, 081406.

(19) Yuan, Z.; Fitzpatrick, M.; Rodgers, L. V. H.; Sangtawesin, S.; Srinivasan, S.; de Leon, N. P. Charge state dynamics and optically detected electron spin resonance contrast of shallow nitrogen-vacancy centers in diamond. *Phys. Rev. Research* **2020**, *2*, 033263.

(20) Bluvstein, D.; Zhang, Z.; Jayich, A. C. B. Identifying and Mitigating Charge Instabilities in Shallow Diamond Nitrogen-Vacancy Centers. *Phys. Rev. Lett.* **2019**, *122*, 076101.

(21) Kawai, S. et al. Nitrogen-Terminated Diamond Surface for Nanoscale NMR by Shallow Nitrogen-Vacancy Centers. *The Journal of Physical Chemistry C* **2019**, *123*, 3594–3604.

(22) Bian, K.; Zheng, W.; Zheng, X.; Chen, X.; Stöhr, R.; Denisenko, A.; Yang, S.; Wrachtrup, J.; Jiang, Y. Nanoscale electric-field imaging based on a quantum sensor and its charge-state control under ambient condition. *Nature Communications* **2021**, *12*, 2457.

(23) Aslam, N.; Waldherr, G.; Neumann, P.; Jelezko, F.; Wrachtrup, J. Photo-induced ionization dynamics of the nitrogen vacancy defect in diamond investigated by single-shot charge state detection. **2013**, *15*, 013064.

(24) Herbschleb, E. D.; Kato, H.; Maruyama, Y.; Danjo, T.; Makino, T.; Yamasaki, S.; Ohki, I.; Hayashi, K.; Morishita, H.; Fujiwara, M.; Mizuochi, N. Ultra-long coherence times amongst room-temperature solid-state spins. *Nature Communications* **2019**, *10*, 3766.

(25) Alkahtani, M.; Hemme, P. Charge stability of nitrogen-vacancy color centers in organic nanodiamonds. *Optical Materials Express* **2020**, *10*, 1224–1231.

(26) Levine, E. V.; Turner, M. J.; Kehayias, P.; Hart, C. A.; Langellier, N.; Trubko, R.; Glenn, D. R.; Fu, R. R.; Walsworth, R. L. Principles and techniques of the quantum diamond microscope. *Nanophotonics* **2019**, *8*, 1945–1973.

(27) Hsu, P.-J.; Rozsa, L.; Finco, A.; Schmidt, L.; Palotas, K.; Vedmedenko, E.; Udvardi, L.; Szunyogh, L.; Kubetzka, A.; Bergmann, K. V.; Wiesendanger, R. Inducing skyrmions in ultrathin Fe films by hydrogen exposure. *Nature Communications* **2018**, *9*, 1571.

(28) Meyer, S.; Perini, M.; von Malottki, S.; Kubetzka, A.; Wiesendanger, R.; von Bergmann, K.; Heinze, S. *Nature Communications* **2019**, *10*, 3823.

(29) Dovzhenko, Y.; Casola, F.; Schlotter, S.; Zhou, T. X.; Büttner, F.; Walsworth, R. L.; Beach, G. S. D.; Yacoby, A. Magnetostatic twists in room-temperatureskyrmions explored by nitrogen-vacancy centerspin texture reconstruction. *Nature Communications* **2018**, *10*, 2712.

(30) Wu, X.; Delbianco, M.; Anggara, K.; Michnowicz, T.; Pardo-Vargas, A.; Bharate, P.; Sen, S.; Pristl, M.; Rauschenbach, S.; Schlickum, U.; Abb, S.; Seeberger, P. H.; Kern, K. Imaging single glycans. *Nature* **2020**, *582*, 375–378.

(31) Anggara, K.; Zhu, Y.; Delbianco, M.; Rauschenbach, S.; Abb, S.; Seeberger, P. H.; Kern, K. Exploring the Molecular Conformation Space by Soft Molecule–Surface Collision. *Journal of American Chemical Society* **2020**, *142*, 21420–21427.

(32) Momenzadeh, S. A.; Stöhr, R. J.; de Oliveira, F. F.; Brunner, A.; Denisenko, A.; Yang, S.; Reinhard, F.; Wrachtrup, J. Nanoengineered Diamond Waveguide as a Robust Bright Platform for Nanomagnetometry Using Shallow Nitrogen Vacancy Centers. *Nano Letters* **2014**, *15*, 165–169.

(33) Santori, C.; Barclay, P. E.; Fu, K.-M. C.; Beausoleil, R. G. Vertical distribution of nitrogen-vacancy centers in diamond formed by ion implantation and annealing. *Phys. Rev. B* **2009**, *79*, 125313.

(34) Schaefer-Nolte, E.; Reinhard, F.; Ternes, M.; Wrachtrup, J.; Kern, K. A diamond-based scanning probe spin sensor operating at low temperature in ultra-high vacuum. *Review of Scientific Instruments* **2014**, *85*, 013701.

(35) Schäfer-Nolte, E. O. Development of a Diamond-based Scanning Probe Spin Sensor Operating at Low Temperature in Ultra High Vacuum. Ph.D. thesis, Universität Stuttgart, 2014.

(36) Janitz, E.; Herb, K.; Völker, L. A.; Huxter, W. S.; Degen, C. L.; Abendroth, J. M. Diamond surface engineering for molecular sensing with nitrogen—vacancy centers. *Journal of Materials Chemistry C* **2022**, *10*, 13533–13569.

(37) Kaviani, M.; Deák, P.; Aradi, B.; Frauenheim, T.; Chou, J.-P.; Gali, A. Proper Surface Termination for Luminescent Near-Surface NV Centers in Diamond. *Nano Letters* **2014**, *14*, 4772–4777.

(38) Kawai, S. et al. Nitrogen-Terminated Diamond Surface for Nanoscale NMR by Shallow Nitrogen-Vacancy Centers. *The Journal of Physical Chemistry C* **2019**, *123*, 3594–3604.

(39) Schreyvogel, C.; Polyakov, V.; Burk, S.; Fedder, H.; Denisenko, A.; Oliveira, F. F.; Wunderlich, R.; Meijer, J.; Zuerbig, V.; Wrachtrup, J.; Nebel, C. E. *Beilstein J. Nanotechnol.* **2016**, *7*, 1727–1735.

(40) Berthel, M.; Mollet, O.; Dantelle, G.; Gacoin, T.; Huant, S.; Drezet, A. Photophysics of single nitrogen-vacancy centers in diamond nanocrystals. *Phys. Rev. B* **2015**, *91*, 035308.

(41) We note that the resulting NV^0 state formed at 4 K, UHV condition, is also a single photon source. However, the LP-650 placed in front of the detection optics (see SI section 1) strongly suppresses any signature from NV^0 in our autocorrelation measurements. This allows us to associate any autocorrelation dip to the presense of a stable NV^- center. Note that the NV^- center is fully recovered only after bringing it back to the NTP measurement stage.

(42) For a comparability of the measurements, we ensured the use of the same laser and microwave power in order to avoid any spurious effects.

(43) Kang, D.; Dai, J.; Yuan, J. Changes of structure and dipole moment of water with temperature and pressure: A first principles study. *Journal of Chemical Physics* **2011**, *135*, 024505.

(44) Lozovoi, A.; Jayakumar, H.; Daw, D.; Vizkelethy, G.; Bielejec, E.; Doherty, M. W.; Flick, J.; Meriles, C. A. Optical activation and detection of charge transport between individual colour centres in diamond. *Nature Electronics* **2021**, *4*, 717–724.

(45) Ishizu, S.; Sasaki, K.; Misonou, D.; Teraji, T.; Itoh, K. M.; Abe, E. Spin coherence and depths of single nitrogen-vacancy centers created by ion implantation into diamond via screening masks. *Journal of Applied Physics* **2020**, *127*, 244502.

(46) Ziegler, J. F.; Ziegler, M.; Biersack, J. SRIM – The stopping and range of ions in matter (2010). *Nuclear Instruments and Methods in Physics Research Section B: Beam Inter-*

actions with Materials and Atoms **2010**, *268*, 1818–1823, 19th International Conference on Ion Beam Analysis.

(47) Momenzadeh, S. A.; Stöhr, R. J.; de Oliveira, F. F.; Brunner, A.; Denisenko, A.; Yang, S.; Reinhard, F.; Wrachtrup, J. Nanoengineered Diamond Waveguide as a Robust Bright Platform for Nanomagnetometry Using Shallow Nitrogen Vacancy Centers. *Nano Letters* **2015**, *15*, 165–169, Publisher: American Chemical Society.

(48) Guo, J.; You, S.; Wang, Z.; Peng, J.; Ma, R.; Jiang, Y. Probing the Structure and Dynamics of Interfacial Water with Scanning Tunneling Microscopy and Spectroscopy. *Journal of visualized experiments : JoVE* **2018**,

(49) Perdew, J. P.; Burke, K.; Ernzerhof, M. Generalized Gradient Approximation Made Simple. *Physical Review Letters* **1996**, *77*, 3865–3868.

(50) Kresse, G.; Furthmüller, J. Efficient iterative schemes for ab initio total-energy calculations using a plane-wave basis set. *Physical Review B* **1996**, *54*, 11169–11186.

(51) Kaviani, M.; Deák, P.; Aradi, B.; Frauenheim, T.; Chou, J.-P.; Gali, A. Proper Surface Termination for Luminescent Near-Surface NV Centers in Diamond. *Nano Letters* **2014**, *14*, 4772–4777.

TOC Graphic

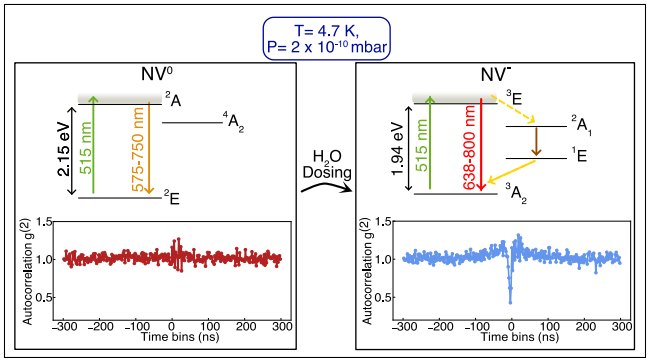
T= 4.7 K,
P= 2 x 10-10 mbar
NV0
2A
4A2
2.15 eV
515 nm
575-750 nm
2E
H2O
Dosing
NV-
3E
2A1
1E
1.94 eV
515 nm
638-800 nm
3A2
Autocorrelation g(2)
1.5
1.0
0.5
-300 -200 -100 0 100 200 300
Time bins (ns)